

# WHAT EFFECTIVE FIELD THEORY MAY CONTRIBUTE TO THE BLAST PROGRAM<sup>a b</sup>

Martin J. Savage

*Department of Physics, University of Washington, Seattle, WA 98195*

Recent progress in using effective field theory to describe two nucleon systems is reviewed.

## 1 Introduction

Several years of effort<sup>1–20</sup> has culminated in a consistent effective field theory description of the nucleon nucleon interaction<sup>17</sup>. The ultimate goal of this endeavour is to construct a framework with which to systematically describe bound and unbound multi-nucleon systems as well as elastic and inelastic processes. This effort was initiated by Weinberg's pioneering work on the subject<sup>1</sup> where he proposed a power-counting scheme for local-operators involving two or more nucleons and the inclusion of pions. However, it was shown that Weinberg's power counting scheme is not consistent. Recently, a consistent power-counting scheme has been proposed<sup>17</sup> to describe  $NN$  scattering and applied to observables of the deuteron. I will focus on these subjects in this talk and give an indication of what this program of study might achieve in the near future.

## 2 Why Effective Field Theory?

Effective field theory is a very powerful technique for dealing with systems that possess widely separated length scales. In a system with just two length scales  $l_1$  and  $l_2$  (as an example), the ratio  $Q = l_1/l_2$  can be used as a small expansion parameter. Usually systems possess more symmetries when  $Q = 0$  and for small  $Q$  a perturbative expansion exists that makes use of the symmetries of the unperturbed system.

In the theory of strong interactions there is one intrinsic length scale,  $\Lambda_{\text{QCD}}$ . For processes that occur at distance scales that are small compared to  $\Lambda_{\text{QCD}}$  the appropriate degrees of freedom are the quarks and gluons with the QCD Lagrange density used to compute processes as a perturbative expansion in the strong interaction coupling constant,  $\alpha_s(\mu)$ . In addition, there is power series expansion in forming the matrix elements of the quark-gluon operators,

---

<sup>a</sup>Talk presented at the *Second Workshop on Electronuclear Physics with Internal Targets and the Bates Large Acceptance Spectrometer Toroid (BLAST)*, May 1998.

<sup>b</sup>NT@UW-18

with an expansion parameter  $\Lambda_{\text{QCD}}/Q$ . It is often useful to impose the constraints of chiral symmetry, arising from the smallness of the light quark masses compared to  $\Lambda_{\text{QCD}}$ , giving yet a third expansion parameter,  $m_q/\Lambda_{\text{QCD}}$ . An explicit example is the semileptonic decay of b-flavored hadrons. The inclusive decay rate for the decay of a  $B$ -meson to a charmed final state is<sup>21</sup>

$$\begin{aligned} \Gamma(B \rightarrow X_c l \bar{\nu}) = & \frac{G_F^2 M_B^5 |V_{cb}|^2}{192\pi^3} 0.369 \left[ 1 - 1.54 \frac{\alpha(m_B)}{\pi} - 1.43 \left( \frac{\alpha(m_B)}{\pi} \right)^2 \beta_0 \right. \\ & - 1.65 \frac{\bar{\Lambda}}{M_B} \left( 1 - 0.87 \frac{\alpha(m_B)}{\pi} \right) \\ & \left. - 0.95 \left( \frac{\bar{\Lambda}}{M_B} \right)^2 - 3.18 \frac{\lambda_1}{M_B^2} + 0.02 \frac{\lambda_2}{M_B^2} \right] . \end{aligned} \quad (1)$$

The quantities  $\bar{\Lambda}$ ,  $\lambda_1$  and  $\lambda_2$  are nonperturbative matrix elements corresponding to the energy of the light degrees of freedom of the  $B$ -meson, the  $b$ -quark fermi-motion and the chromomagnetic interaction between the  $b$ -quark and the light degrees of freedom, respectively. In contrast, for processes at intermediate length scales there are no small expansion parameters. The strong interaction coupling  $\alpha_s(\mu)$  is approaching unity, as is  $\Lambda_{\text{QCD}}/Q$ . At long distances the appropriate degrees of freedom are the hadrons themselves, and not the quark and gluon fields.  $U(1)_{\text{em}}$  gauge symmetry of electromagnetism, the  $SU(2)_L \otimes SU(2)_R$  chiral symmetry and the small expansions parameters  $\mathbf{p}/\Lambda$  and  $m_q/\Lambda$  (where  $\mathbf{p}$  denote the external momentum of the hadrons,  $m_q$  are the light quark masses and  $\Lambda$  is the scale of strong interactions) can be incorporated a Lagrange density describing the low energy dynamics of hadrons and photons.

Writing the Lagrange density as

$$\mathcal{L} \left( \frac{\mathbf{p}}{\Lambda}, \frac{m_q}{\Lambda} \right) = \sum_i C^{(i)}(\mu) \mathcal{O}^{(i)}(\mu) \quad , \quad (2)$$

where the operators  $\mathcal{O}^{(i)}(\mu)$  are renormalized at the scale  $\mu$  and are constructed from the hadronic fields. Coefficients  $C^{(i)}(\mu)$  renormalized at  $\mu$  are determined by the short-distance behavior of the strong interactions. Clearly eq.(2) represents an explicit separation of scales. By construction, observables do not depend upon the scale  $\mu$  at which one chooses to renormalize. Initially, this appears to be a disastrous situation, since there are an infinite number of operators that one can construct and hence there are an infinite number of constants unconstrained by the symmetries of the theory. However, we have

learned much about dealing with non-renormalizable field theories over the last many years and in general such theories are predictive. To construct relations between certain observables that are valid to a certain precision, only a finite number of constants in the effective Lagrange density need to be determined. The key to making such theories predictive is to establish a consistent power counting scheme, one in which terms that “look small” at the level of the lagrange density do in fact make small contributions to observables, even with the inclusion of loop effects.

### 3 The $NN$ Interaction and Weinberg’s Power Counting

The most general Lagrange density consistent with chiral symmetry describing the interaction of two nucleons is

$$\begin{aligned} \mathcal{L} = & N^\dagger(iD_0 + \vec{D}^2/2M)N + \frac{f^2}{8}\text{Tr} \partial_\mu \Sigma^\dagger \partial^\mu \Sigma + \frac{f^2}{4}\omega \text{Tr} m_q(\Sigma + \Sigma^\dagger) \\ & - \frac{1}{2}C_S(N^\dagger N)^2 - \frac{1}{2}C_T(N^\dagger \vec{\sigma} N)^2 + g_A N^\dagger \vec{A} \cdot \vec{\sigma} N + \dots \quad , \end{aligned} \quad (3)$$

where  $D_\mu$  denotes a chiral-covariant derivative and  $\Sigma$  is the exponential of the isotriplet of pions

$$\begin{aligned} \Sigma &= \exp\left(\frac{2i}{f}M\right) \\ M &= \begin{pmatrix} \pi^0/\sqrt{2} & \pi^+ \\ \pi^- & -\pi^0/\sqrt{2} \end{pmatrix} \quad , \end{aligned} \quad (4)$$

with  $f = 132$  MeV the pion decay constant and  $\vec{A}$  is the axialvector meson field. The ellipses denote terms with more spatial derivatives and more insertions of the light quark mass matrix,  $m_q$ . The Georgi-Manohar<sup>22</sup> naive dimensional analysis arising from a consideration of loop contributions to observables suggests that  $C_{S,T} \sim 1/f^2$ , and Weinberg’s power-counting will follow directly.

A necessary ingredient for an EFT is a power counting scheme that dictates which graphs to compute in order to determine an observable to a desired order in the expansion. We denote the expansion parameters of the theory by  $Q \sim |\mathbf{p}|, m_q^{1/2}$ . The main complication in the theory of nucleons and pions is the fact that a nucleon propagator  $S(q) = i/(q_0 - \mathbf{q}^2/2M)$  scales like  $1/Q$  if  $q_0$  scales like  $m_\pi$  or an external 3-momentum, while  $S(q) \sim M/Q^2$  if  $q_0$  scales like an external kinetic energy. Similarly, in loops  $\int dq_0$  can scale like  $Q$  or  $Q^2/M$ , depending on which pole is picked up. To distinguish between these two scaling properties it is convenient to define generalized “ $n$ -nucleon

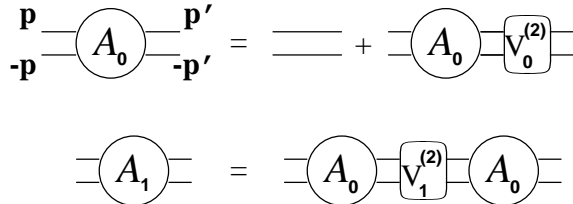


Figure 1: The first two terms in the EFT expansion of the Feynman amplitude for nucleon-nucleon scattering in Weinberg’s power-counting scheme. The leading amplitude  $\mathcal{A}_0$  consists of the sum of ladder diagrams with the leading 2-nucleon potential  $V_0^{(2)}$  at every rung.

potentials”  $V^{(n)}$  comprised of those parts of connected Feynman diagrams with  $2n$  external nucleon lines that have no powers of  $M$  in their scaling (except from relativistic corrections).  $V^{(n)}$  includes diagrams which are  $n$ -nucleon irreducible and parts of diagrams which are 1-nucleon irreducible. To compute the latter contribution to  $V^{(n)}$  one identifies all combinations of two or more internal nucleon lines that can be simultaneously on-shell, and excludes their pole contributions when performing the  $\int dq_0$  loop integrations.

Two nucleon scattering is simple since the graphs are all ladder diagrams with insertions of  $V^{(2)}$ ’s acting as ladder rungs. Each loop of the ladder introduces a loop integration ( $dq_0 d^3\mathbf{q} \sim Q^5/M$ ) and two nucleon propagators ( $M^2/Q^4$ ) to give a factor of  $(QM)$  per loop. If one treats  $M \simeq Q^0$ , it follows that perturbation theory is adequate for describing the 2-nucleon system at low  $Q$ . In order to accommodate large scattering lengths and bound states near threshold, as in the  $^1S_0$  and  $^3S_1 - ^3D_1$  channels one must conclude that  $M \sim 1/Q$  in this power counting scheme. At leading order one must sum up all ladder diagrams with insertions of the leading two-body potential  $V_0^{(2)}$ , while at subleading order one includes one insertion of the subleading potential,  $V_1^{(2)}$  and all powers of  $V_0^{(2)}$ , and so forth.

At leading order in Weinbergs power-counting there are contributions to  $V_0^{(2)}$  from both the local four-nucleon operators,  $C_{S,T}$  and from the exchange of a single potential pion, giving a momentum space potential of

$$V_0^{(2)}(\mathbf{p}, \mathbf{p}') = C - \left( \frac{g_A^2}{2f_\pi^2} \right) \frac{(\mathbf{q} \cdot \sigma_1 \mathbf{q} \cdot \sigma_2)(\tau_1 \cdot \tau_2)}{(\mathbf{q}^2 + m_\pi^2)} \quad , \quad (5)$$

where  $C$  denotes the combination of  $C_{S,T}$  appropriate for a given spin-isospin channel. The leading order amplitude results from summing the graphs shown in Fig. (1) resulting from this potential, i.e. solving the Schrodinger equation.

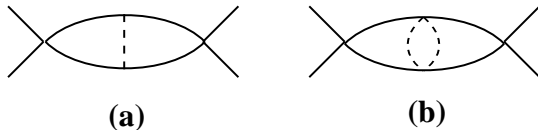


Figure 2: Graphs with logarithmic divergences. The divergence in graph (a) is proportional to  $M^2 m_\pi^2$ , while graph (b) has a divergence proportional to  $M^2 \mathbf{p}^4$ . The solid lines are nucleons and the dashed lines are pions.

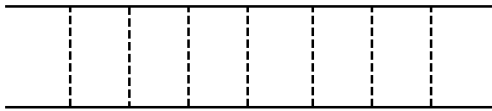


Figure 3: A contribution to the pion ladder sum, arising at leading order in Weinberg's power-counting. The solid lines are nucleons and the dashed lines are pions.

In the  ${}^1S_0$  channel at two-loops in the ladder sum there is a logarithmic divergence in the graph shown in Fig. (2a) that must be regulated. In dimensional regularization the divergent part of this graph is

$$-\frac{1}{\epsilon} \frac{g_A^2 m_\pi^2 M^2}{128\pi^2 f_\pi^2} C^2, \quad (6)$$

which requires a counterterm with a single insertion of the light quark mass matrix. However, the coefficients of these operators must scale like  $M^2$ , and since  $m_\pi^2 M^2 \sim Q^0$  these formally higher order operators in Weinberg's power-counting are required at leading order to absorb divergences in the time-ordered products of the leading order potential,  $V_0^{(2)}$ . Ignoring the multi-pion vertices arising from these operators, they can be re-absorbed into the leading operators with coefficients  $C_{S,T}$ .

The situation is different in the  ${}^3S_1 - {}^3D_1$  channel and in higher partial waves. A contribution to the leading order ladder sum is shown in Fig. (3), arising from seven potential pion exchanges, i.e a six-loop graph. It is straightforward to deduce that this graph has a logarithmic divergence at order  $(QM)^6$ , and therefore, counterterms involving  $\nabla^6$  are required at leading order in the expansion. Clearly, the same discussion can be made for an arbitrary number of potential pion exchanges, and therefore counterterms involving an arbitrary even number of  $\nabla$ 's are required. This is a clear demonstration of the failure of Weinberg's power-counting. Further, this conclusion is true for all regularization schemes and not just for dimensional regularization.

#### 4 A New Power Counting

Lets us begin by examining the general form of the amplitude for nucleon scattering in a S-wave

$$\mathcal{A} = \frac{4\pi}{M} \frac{1}{p \cot \delta - ip} \quad . \quad (7)$$

From quantum mechanics it is well known that  $p \cot \delta$  has a momentum expansion for  $p \ll \Lambda$  (the effective range expansion),

$$p \cot \delta = -\frac{1}{a} + \frac{1}{2}\Lambda^2 \sum_{n=0}^{\infty} r_n \left(\frac{p^2}{\Lambda^2}\right)^{n+1} \quad , \quad (8)$$

where  $a$  is the scattering length, and  $r_0$  is the effective range. For scattering in the  $^1S_0$  and  $^3S_1$  channels the scattering lengths are found to be large,  $a(^1S_0) = -23.714 \pm 0.013$  fm and  $a(^3S_1) = +5.425 \pm 0.0014$  fm respectively. Expanding the expression for the amplitude in eq.(7) in powers of  $p/\Lambda$  while retaining  $ap$  to all orders gives

$$\mathcal{A} = -\frac{4\pi}{M} \frac{1}{(1/a + ip)} \left[ 1 + \frac{r_0/2}{(1/a + ip)} p^2 + \frac{(r_0/2)^2}{(1/a + ip)^2} p^4 + \frac{(r_1/2\Lambda^2)}{(1/a + ip)} p^4 + \dots \right] \quad (9)$$

For  $p > 1/|a|$  the terms in this expansion scale as  $\{p^{-1}, p^0, p^1, \dots\}$ , and the expansion in the effective theory takes the form

$$\mathcal{A} = \sum_{n=-1}^{\infty} \mathcal{A}_n \quad , \quad \mathcal{A}_n \sim p^n \quad . \quad (10)$$

In the theory without pions we can explicitly compute the s-wave amplitude in each spin channel to all orders in the momentum expansion,

$$\mathcal{A} = -\frac{\sum C_{2n} p^{2n}}{1 + M(\mu + ip)/4\pi \sum C_{2n} p^{2n}} \quad , \quad (11)$$

where  $C_{2n}$  is the coefficient of the  $p^{2n}$  term in the lagrange density.  $\mu$  is the renormalization scale and we have used Power Divergence Subtraction (PDS)<sup>17</sup> to define the theory. A typical loop graph that appears in the amplitude has the form

$$\begin{aligned} I_n &\equiv -i \left(\frac{\mu}{2}\right)^{4-D} \int \frac{d^D q}{(2\pi)^D} \mathbf{q}^{2n} \left( \frac{i}{\frac{E}{2} + q_0 - \frac{\mathbf{q}^2}{2M} + i\epsilon} \right) \left( \frac{i}{\frac{E}{2} - q_0 - \frac{\mathbf{q}^2}{2M} + i\epsilon} \right) \\ &= -M(ME)^n (-ME - i\epsilon)^{(D-3)/2} \Gamma\left(\frac{3-D}{2}\right) \frac{\left(\frac{\mu}{2}\right)^{4-D}}{(4\pi)^{(D-1)/2}} \quad , \quad (12) \end{aligned}$$

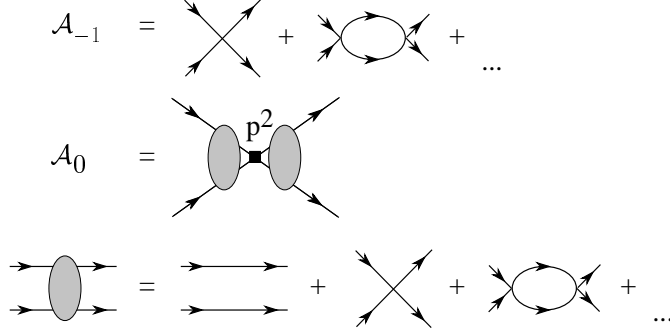


Figure 4: Leading and subleading contributions arising from local operators.

where  $D$  is the number of space-time dimensions. In the *PDS* scheme the pole at  $D = 3$  is removed by adding a local counterterm to the lagrange density, so that the sum of the loop graph and counterterm in  $D = 4$  dimensions is

$$I_n^{PDS} = I_n + \delta I_n = -(ME)^n \left( \frac{M}{4\pi} \right) (\mu + ip). \quad (13)$$

The amplitude  $\mathcal{A}$  is independent of the subtraction point  $\mu$  and this determines the  $\mu$  dependence of the coefficients,  $C_{2n}$ . In the *PDS* scheme one finds that for  $\mu \gg 1/|a|$ , the couplings  $C_{2n}(\mu)$  scale as

$$C_{2n}(\mu) \sim \frac{4\pi}{M\Lambda^n \mu^{n+1}}, \quad (14)$$

so that if we take  $\mu \sim p$ ,  $C_{2n}(\mu) \sim 1/p^{n+1}$ . A factor of  $\nabla^{2n}$  at a vertex scales as  $p^{2n}$ , while each loop contributes a factor of  $p$ . Therefore, the leading order contribution to the scattering amplitude  $\mathcal{A}_{-1}$  scales as  $p^{-1}$  and consists of the sum of bubble diagrams with  $C_0$  vertices. Contributions scaling as higher powers of  $p$  come from perturbative insertions of derivative interactions, dressed to all orders by  $C_0$ . The first two terms in the expansion

$$\mathcal{A}_{-1} = \frac{-C_0}{\left[1 + \frac{C_0 M}{4\pi} (\mu + ip)\right]} \quad , \quad \mathcal{A}_0 = \frac{-C_2 p^2}{\left[1 + \frac{C_0 M}{4\pi} (\mu + ip)\right]^2} \quad , \quad (15)$$

correspond to the Feynman diagrams in Fig. (4). A comparison with eq.(9)

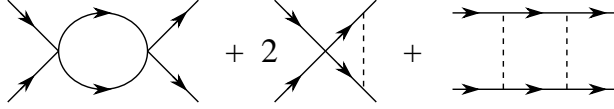


Figure 5: Contributions to the  $\beta$ -functions for  $C_0$  in the theory with pions

gives

$$C_0(\mu) = \frac{4\pi}{M} \left( \frac{1}{-\mu + 1/a} \right) \quad , \quad C_2(\mu) = \frac{4\pi}{M} \left( \frac{1}{-\mu + 1/a} \right)^2 \frac{r_0}{2} \quad . \quad (16)$$

The dependence of  $C_{2n}(\mu)$  on  $\mu$  is determined by requiring the amplitude be independent of the renormalization scale  $\mu$ . The physical parameters  $a$ ,  $r_n$  enter as boundary conditions on the resulting renormalization group (RG) equations. In general one finds the coefficients to be

$$C_{2n}(\mu) = \frac{4\pi}{M(-\mu + 1/a)} \left( \frac{r_0/2}{-\mu + 1/a} \right)^n + O(\mu^{-n}) \quad , \quad (17)$$

which has the scaling property in eq.(14). The leading behavior depends on the two parameters  $a$  and  $r_0$  encountered when solving for  $C_0(\mu)$  and  $C_2(\mu)$ . This is due to the  $C_{2n}$  couplings being driven primarily by lower dimensional interactions.

The inclusion of pions into the theory is straightforward. While the coefficients of the local operators are renormalized, and scale as powers of the renormalization scale  $\mu$  (we use  $Q \equiv \mu \sim p \sim m_q^{1/2}$ ), the exchange of a single potential pion does not suffer from such renormalizations and therefore pion exchange is a sub-leading contribution,  $Q^0$ . At the same order as the exchange of a potential pion is an insertion of a  $C_2$  operator and a single insertion of the quark mass matrix  $m_q$ . Ignoring isospin violation, these operators involving insertions of the light quark mass matrix with coefficients  $D_2$  have the same structure as the  $C_0$  operators. For  $\mu \sim m_\pi$ ,  $C_0(\mu) \propto 1/\mu$ ,  $C_2(\mu) \propto 1/\mu^2$  and  $D_2(\mu) \propto 1/\mu^2$  for the  $^1S_0$  and  $^3S_1$  channels. A feature of the theory with pions is that this scaling behavior breaks down at low momentum,  $p \sim 1/|a|$ , and at sufficiently high momentum. Solving the RG equation arising from the graphs shown in Fig. (5) in the  $^1S_0$  channel with the boundary condition  $C_0^{(^1S_0)}(0) = 4\pi a_1/M$ , where  $a_1$  is the  $^1S_0$  scattering length, we find for  $\mu \gg 1/|a_1|$

$$C_0^{(^1S_0)}(\mu) \simeq -\frac{4\pi}{M\mu} \left( 1 + \frac{\mu}{\Lambda_{NN}} \right) \quad , \quad (18)$$



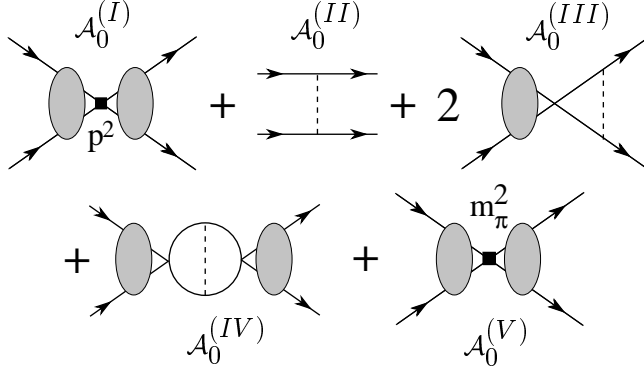


Figure 6: Graphs contributing to the subleading amplitude  $\mathcal{A}_0$ . The shaded ovals are defined in Fig. (4).

with

$$\Lambda_{NN} = \frac{8\pi f^2}{g_A^2 M} \sim 300 \text{ MeV} \quad , \quad (19)$$

and therefore the power counting changes when  $\mu \sim \Lambda_{NN}$ . The UV fixed point toward which  $C_0^{(1S_0)}$  is driven largely cancels the  $\delta$ -function component of the single potential pion exchange in the  $^1S_0$  channel. As a result, this power counting is valid up to  $p \sim \Lambda_{NN}$  and the power counting in both channels is expected to fail at momenta on the order of  $\Lambda_{NN}$ . We conclude that the expansion parameter for this theory is  $\sim m_\pi/\Lambda_{NN} \sim \frac{1}{2}$ , larger than one would like.

## 5 NN scattering in the $^1S_0$ Channel

Having established a consistent power-counting in the previous sections we now apply it to  $NN$  scattering in the  $^1S_0$  channel. The amplitude at order  $Q^{-1}$  and  $Q^0$  determined from the graphs shown in Fig. (4) and Fig. (6) are

$$\mathcal{A}_{-1} = -\frac{C_0^{(1S_0)}}{1 + C_0^{(1S_0)} \frac{M}{4\pi} (\mu + ip)} \quad ,$$

$$\mathcal{A}_0^{(I)} = -C_2^{(1S_0)} p^2 \left[ \frac{\mathcal{A}_{-1}}{C_0^{(1S_0)}} \right]^2 \quad ,$$

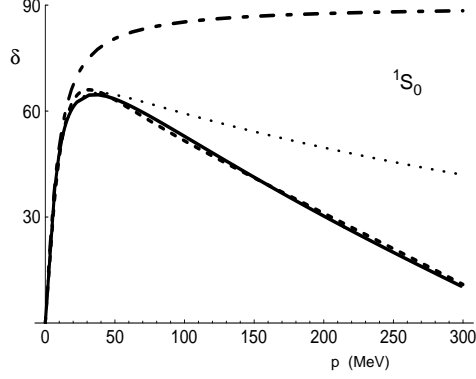


Figure 7: The phase shift  $\delta$  for the  $^1S_0$  channel. The dot-dashed curve is the one parameter fit at order  $Q^{-1}$ , that reproduces the scattering length. The dashed curve corresponds to fitting  $\delta$  between  $0 < p < 200$  MeV, while the dotted curve corresponds to fitting the scattering length and effective range. The solid line shows the results of the Nijmegen partial wave analysis.

$$\begin{aligned}
\mathcal{A}_0^{(II)} &= \left( \frac{g_A^2}{2f^2} \right) \left( -1 + \frac{m_\pi^2}{4p^2} \ln \left( 1 + \frac{4p^2}{m_\pi^2} \right) \right) \quad , \\
\mathcal{A}_0^{(III)} &= \frac{g_A^2}{f^2} \left( \frac{m_\pi M \mathcal{A}_{-1}}{4\pi} \right) \left( -\frac{(\mu + ip)}{m_\pi} + \frac{m_\pi}{2p} X(p, m_\pi) \right) \quad , \\
\mathcal{A}_0^{(IV)} &= \frac{g_A^2}{2f^2} \left( \frac{m_\pi M \mathcal{A}_{-1}}{4\pi} \right)^2 \left( 1 - \left( \frac{\mu + ip}{m_\pi} \right)^2 + iX(p, m_\pi) - \ln \left( \frac{m_\pi}{\mu} \right) \right) \quad , \\
\mathcal{A}_0^{(V)} &= -D_2^{(^1S_0)} m_\pi^2 \left[ \frac{\mathcal{A}_{-1}}{C_0^{(^1S_0)}} \right]^2 \quad , \\
X(p, m_\pi) &= \tan^{-1} \left( \frac{2p}{m_\pi} \right) + \frac{i}{2} \ln \left( 1 + \frac{4p^2}{m_\pi^2} \right) \quad . \tag{20}
\end{aligned}$$

At order  $Q^{-1}$  there is one unknown coefficient  $C_0^{(^1S_0)}$  that must be determined from data while at order  $Q^0$  there are three unknown coefficients  $C_0^{(^1S_0)}$ ,  $C_2^{(^1S_0)}$  and  $D_2^{(^1S_0)}$  that must be determined. The graph giving  $\mathcal{A}_0^{(IV)}$  is divergent in four dimensions and therefore gives rise to the logarithmic dependence on the renormalization scale  $\mu$  in eq. (20). In order for the expansion to converge, the leading term  $\mathcal{A}_{-1}$  must capture most of the scattering length. The phase shift  $\delta$  is perturbatively expanded in  $Q$ ,  $\delta = \delta^{(0)} + \delta^{(1)} + \dots$  and fit to the results of

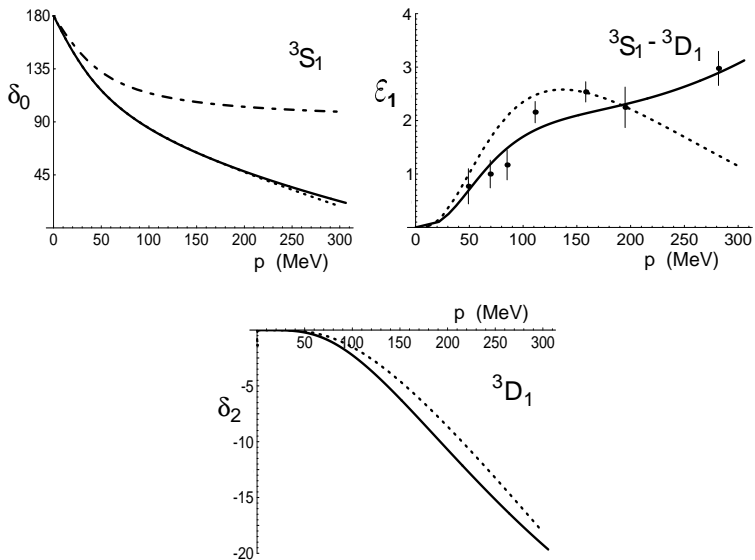


Figure 8: The phase shifts  $\delta_0$ ,  $\delta_2$  and mixing parameter  $\epsilon_1$  for the  ${}^3S_1 - {}^3D_1$  channel. The solid line denotes the results of the Nijmegen partial wave analysis. The dot-dashed curve is the fit at order  $Q^{-1}$  for  $\delta_0$ , while  $\delta_2 = \epsilon_1 = 0$  at this order. The dashed curves are the results of the order  $Q^0$  fit of  $\delta_0$  to the partial wave analysis over the momentum range  $p \leq 200$  MeV.

the Nijmegen partial-wave analysis<sup>23</sup> over a momentum range  $p \leq 200$  MeV. We find for  $\mu = m_\pi$

$$C_0^{({}^1S_0)} = -3.34 \text{ fm}^2, \quad D_2^{({}^1S_0)} = -0.42 \text{ fm}^4, \quad C_2^{({}^1S_0)} = 3.24 \text{ fm}^4, \quad (21)$$

giving the dashed curve plotted in Fig. (7). It is clear from Fig. (7) that the corrections to the leading order result become substantial above  $\sim 200$  MeV and we expect the expansion to become unreliable at momenta larger than this value. We chose to renormalize at  $\mu = m_\pi$  for our numerical analysis, but we could have chosen any value of  $\mu$ , with  $\Lambda_{NN} \gg \mu \gg 1/a$ . The logarithm appearing in the subleading amplitude suggests we choose  $\mu \sim m_\pi$ .

## 6 NN scattering in the ${}^3S_1 - {}^3D_1$ Channel

The analysis of scattering in the  ${}^3S_1 - {}^3D_1$  channel is a straightforward extension of the analysis in the  ${}^1S_0$  channel. The important difference is that the nucleons

in the initial and final states with total angular momentum  $J = 1$  can be in an orbital angular momentum state of either  $L = 0$  or  $L = 2$ . The power counting for amplitudes that take the nucleons from a  ${}^3S_1$ -state to a  ${}^3S_1$ -state is identical to the analysis in the  ${}^1S_0$ -channel. Operators between two  ${}^3D_1$  states are not directly renormalized by the leading operators, which project out only  ${}^3S_1$  states. However, they are renormalized by operators that mix the  ${}^3S_1$  and  ${}^3D_1$  states, which in turn are renormalized by the leading interactions. Further, they involve a total of four spatial derivatives, two on the incoming nucleons, and two on the out-going nucleons. Therefore, such operators contribute at order  $Q^3$ , and can be neglected in the present computation. Consequently, amplitudes for scattering from an  ${}^3D_1$  state into an  ${}^3D_1$  state are dominated by single potential pion exchange at order  $Q^0$ . Operators connecting  ${}^3D_1$  and  ${}^3S_1$  states are renormalized by the leading operators, but only on the  $L = 0$  “side” of the operator. Therefore the coefficient of this operator,  $C_2^{({}^3S_1-{}^3D_1)} \sim 1/\mu$ , contributing at order  $Q^1$  and it can be neglected at order  $Q^0$ . Thus, mixing between  ${}^3D_1$  and  ${}^3S_1$  states is dominated by single potential pion exchange dressed by a bubble chain of  $C_0^{({}^3S_1)}$  operators and a parameter free prediction for this mixing exists at order  $Q^0$ . Fitting the parameters  $C_0^{({}^3S_1)}$ ,  $C_2^{({}^3S_1)}$  and  $D_2^{({}^3S_1)}$  to the phase shift  $\delta_0$  over the momentum range  $p \leq 200$  MeV yields, at  $\mu = m_\pi$

$$C_0^{({}^3S_1)} = -5.51 \text{ fm}^2, \quad D_2^{({}^3S_1)} = 1.32 \text{ fm}^4, \quad C_2^{({}^3S_1)} = 9.91 \text{ fm}^4. \quad (22)$$

The dashed curves in Fig. (8) show the phase shifts  $\delta_0$ ,  $\delta_2$  and mixing parameter  $\varepsilon_1$  compared to the Nijmegen partial wave analysis<sup>23</sup> for this set of coefficients. There are no free parameters at this order in either  $\varepsilon_1$  or  $\delta_2$  once  $C_0^{({}^3S_1)}$  has been determined from  $\delta_0$ .

## 7 The Deuteron

Once the Lagrange density in the nucleon sector has been established the standard tools of field theory can be used to determine the properties of the deuteron<sup>17</sup>. To compute the electromagnetic form factors of the deuteron one first computes the three point correlation function between a source that creates a nucleon pair in a  ${}^3S_1$  state, a source that destroys a nucleon pair in a  ${}^3S_1$  state and a source that creates a photon. After LSZ reduction and wavefunction renormalization one obtains the electromagnetic form factors. Leading, subleading and subsubleading order graphs contributing to the electric form factors of the deuteron are shown in Fig. (9). The resulting form factors  $A(q^2)$  and  $B(q^2)$  that appear in the differential cross section for electron deuteron

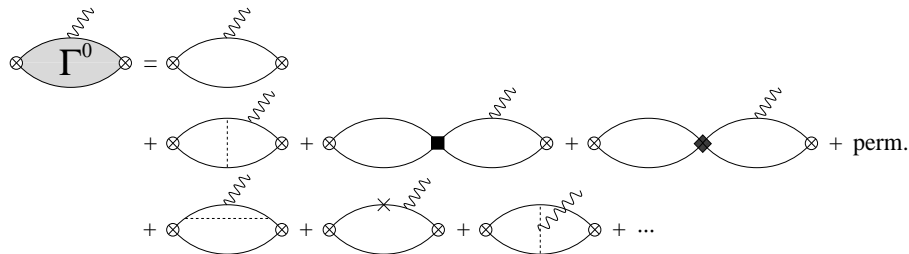


Figure 9: The diagrams contributing to the electric form factors of the deuteron.

scattering are shown in Fig. (10).  $A(q^2)$  is dominated by the charge form factor and  $B(q^2)$  depends only upon the magnetic form factor. One sees that the form factors computed at subleading order agree well with the data. The charge radius of the deuteron is found to be

$$\begin{aligned}
 \sqrt{\langle r^2 \rangle_{\text{th}}} &= \frac{1}{2\sqrt{2}\gamma} + C_2(\mu) \frac{M(\mu - \gamma)^2}{48\sqrt{2}\pi} + \frac{g_A^2 M m_\pi^2 (3m_\pi + 10\gamma)}{288\sqrt{2}\pi f_\pi^2 (m_\pi + 2\gamma)^3} + \dots \\
 &= 1.89 \text{ fm} + \dots \\
 \sqrt{\langle r^2 \rangle_{\text{expt}}} &= 1.963 \text{ fm} \quad , \quad (23)
 \end{aligned}$$

where  $\gamma = \sqrt{M_N B}$  is the binding momentum of the deuteron. The result computed to subleading order agrees with the observed value. The quadrupole moment vanishes at leading order in the expansion but receives a contribution at subleading order from the exchange of one potential pion, giving

$$\begin{aligned}
 \mu_{\mathcal{Q},\text{th}} &= \frac{g_A^2 M (6MB + 9m_\pi \gamma + 4m_\pi^2)}{30\pi f_\pi^2 (m_\pi + 2\gamma)^3} + \dots \\
 &= 0.40 \text{ fm}^2 + \dots \\
 \mu_{\mathcal{Q},\text{expt}} &= 0.2859 \text{ fm}^2 \quad , \quad (24)
 \end{aligned}$$

which is approximately 30% larger than the experimental value. Clearly, a subsubleading calculation is needed to ensure that the theoretical value is converging to the experimental value. This work is currently in progress<sup>25</sup>. In contrast, there is a local counterterm contributing to the magnetic moment at subleading order. We find

$$\begin{aligned}
 \mu_M &= \mu_p + \mu_n + L_2(\mu) \frac{\gamma}{2\pi} (\mu - \gamma)^2 + \dots \\
 &= 0.88 - 0.02 \text{ (fit)} \quad , \quad (25)
 \end{aligned}$$

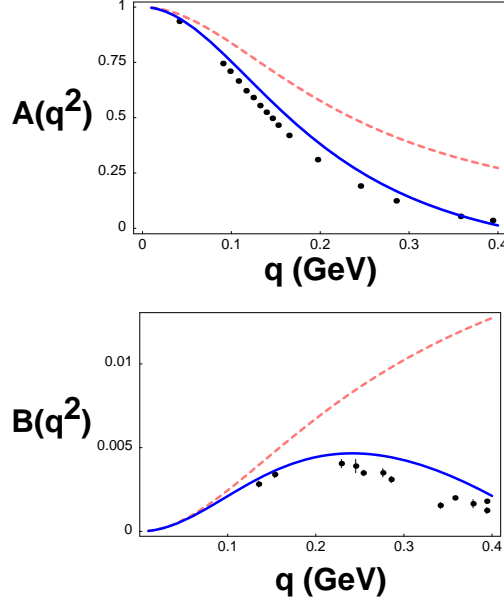


Figure 10: The form factors  $A(q^2)$  and  $B(q^2)$  measured in elastic electron-deuteron scattering. The dashed curve is the leading order prediction, while the solid curve subleading prediction. There is one counterterm in  $B(q^2)$  that is fixed by the deuteron magnetic moment.

which determines the counterterm  $L_2$  at the scale  $\mu$ . Once this counterterm is determined from the deuteron magnetic moment, the entire form factor  $B(q^2)$  is determined to subleading order.

We have also computed the polarizabilities of the deuteron<sup>26</sup>, and find that the scalar  $\alpha_{E0}$  and tensor  $\alpha_{E2}$  electric polarizabilities, are

$$\begin{aligned}
\alpha_{E0} &= \frac{\alpha M_N}{32\gamma^4} + \frac{\alpha M_N^2}{64\pi\gamma^3} C_2(\mu)(\mu - \gamma)^2 \\
&+ \frac{\alpha g_A^2 M_N^2}{384\pi f^2} \frac{m_\pi^2(3m_\pi^2 + 16m_\pi\gamma + 24\gamma^2)}{\gamma^3(m_\pi + 2\gamma)^4} + \dots \\
\alpha_{E2} &= -\frac{\alpha g_A^2 M_N^2}{80\pi f^2} \frac{2m_\pi^3 + 11m_\pi^2\gamma + 16m_\pi\gamma^2 + 8\gamma^3}{\gamma^2(m_\pi + 2\gamma)^4} \\
\alpha_{E0} &= 0.595 \text{ fm}^3 + \dots, \quad \alpha_{E2} = -0.062 \text{ fm}^3 + \dots, \quad (26)
\end{aligned}$$

while the scalar and tensor magnetic polarizabilities,  $\beta_{M0}$  and  $\beta_{M2}$ , are

$$\begin{aligned}\beta_{M0} &= \frac{\alpha}{2M_N} \left[ -\frac{1}{16\gamma^2} + \frac{2(\kappa^{(0)})^2 + (\kappa^{(1)})^2}{3\gamma^2} + \frac{(\kappa^{(1)})^2}{6\pi} \frac{M_N}{\gamma} \mathcal{A}_{-1}^{(1S_0)}(-B) \right] \\ \beta_{M2} &= -\frac{\alpha}{M_N} \frac{(\kappa^{(0)})^2 - (\kappa^{(1)})^2}{2\gamma^2} + \frac{\alpha(\kappa^{(1)})^2}{4\pi\gamma} \mathcal{A}_{-1}^{(1S_0)}(-B) \\ \beta_{M0} &= 0.067 \text{ fm}^3 + \dots \quad , \quad \beta_{M2} = 0.195 \text{ fm}^3 + \dots \quad ,\end{aligned}\tag{27}$$

where  $\mathcal{A}_{-1}^{(1S_0)}(E)$  is the scattering amplitude in the  $^1S_0$  channel evaluated at a center of mass energy  $E$ .  $\kappa^{(0)}$  and  $\kappa^{(1)}$  are the isoscalar and isovector magnetic moments of the nucleon respectively.

## 8 Present Limitations

The power counting fails at the scale  $\Lambda_{NN}$  and there has been little progress in understanding how to deal momentum higher than  $\Lambda_{NN}$  in the effective field theory framework. Therefore we are presently unable to address some important areas, such as photo-pion production off the deuteron or elastic pion deuteron scattering. The typical momentum scale in such a process is  $\sim \sqrt{M_N m_\pi}$  greater than  $\Lambda_{NN}$ .

It is also worth commenting on the role of baryonic resonances in this program. The impact of the  $\Delta$  resonance has been determined in Weinberg's power-counting scheme in two different prescriptions<sup>2,9</sup> <sup>c</sup>. It is found not to play an important role in  $NN$  scattering as the mass scale that sets the size of its contribution is  $\sqrt{M(M_\Delta - M)} \sim 500$  MeV. This scale is higher than the scale at which the power counting becomes inappropriate,  $\Lambda_{NN}$ , and so the baryonic resonances should not be included, until the theory above the scale  $\Lambda_{NN}$  is constructed.

## 9 Conclusions

After several years of investigation we have constructed a consistent power counting for an effective field theory description of the nucleon nucleon interaction<sup>17</sup>. Pions are subleading compared to the local momentum independent four-nucleon operators and can be treated in perturbation theory.  $NN$  scattering in the  $^1S_0$  and  $^3S_1 - ^3D_1$  channels to sub-leading order has been considered and most impressive perhaps is the parameter-free prediction of the  $^3S_1 - ^3D_1$  mixing parameter  $\varepsilon_1$  which agrees reasonably well with the Nijmegen phase

<sup>c</sup>The  $\Delta(1232)$  and other baryon resonances have been consistently included in the single nucleon sector<sup>24</sup>.

shift analysis. The properties of the deuteron bound state follow straightforwardly from this construction. I presented the electromagnetic form factors and polarizabilities. One of the nice features of having a field theory construction is that there are many well known theorems. One such theorem<sup>27,28</sup> is that contributions from operators that vanish by the equations of motion are of the form of higher dimension operators that do not vanish by the equations of motion and therefore such operators can be neglected.

The future looks extremely promising for a systematic analysis of nuclear physics using effective field theory. The short term program will be to continue to examine the two-body systems in detail, working to higher orders in the effective field theory expansion. In the long-term one hopes to make progress in three-body<sup>44</sup> and higher-body systems. Both lines of investigation are directly relevant to the BLAST program, and I look forward to close cooperation between experimental and theoretical endeavours in this area.

I would like to thank the organizers Ricardo Alarcon and Richard Milner for putting together such a stimulating meeting. This work is supported in part by Department of Energy Grant DE-FG03-97ER41014.

## References

1. S. Weinberg, *Phys. Lett. B* **251**, 288 (1990); *Nucl. Phys. B* **363**, 3 (1991); *Phys. Lett. B* **295**, 114 (1992).
2. C. Ordonez and U. van Kolck, *Phys. Lett. B* **291**, 459 (1992); C. Ordonez, L. Ray and U. van Kolck, *Phys. Rev. Lett.* **72**, 1982 (1994) ; *Phys. Rev. C* **53**, 2086 (1996) ; U. van Kolck, *Phys. Rev. C* **49**, 2932 (1994) .
3. T.S. Park, D.P. Min and M. Rho, *Phys. Rev. Lett.* **74**, 4153 (1995) ; *Nucl. Phys. A* **596**, 515 (1996).
4. D.B. Kaplan, M.J. Savage and M.B. Wise, *Nucl. Phys. B* **478**, 629 (1996).
5. T. Cohen, J.L. Friar, G.A. Miller and U. van Kolck, *Phys. Rev. C* **53**, 2661 (1996).
6. D. B. Kaplan, *Nucl. Phys. B* **494**, 471 (1997).
7. T.D. Cohen, *Phys. Rev. C* **55**, 67 (1997). D.R. Phillips and T.D. Cohen, *Phys. Lett. B* **390**, 7 (1997). K.A. Scaldferri, D.R. Phillips, C.W. Kao and T.D. Cohen, *Phys. Rev. C* **56**, 679 (1997). S.R. Beane, T.D. Cohen and D.R. Phillips, nucl-th/9709062.
8. J.L. Friar, *Few Body Syst.* **99**, 1 (1996).
9. M.J. Savage, *Phys. Rev. C* **55**, 2185 (1997).



10. M. Luke and A.V. Manohar, *Phys. Rev. D* **55**, 4129 (1997).
11. G.P. Lepage, [nucl-th/9706029](#), Lectures at 9th Jorge Andre Swieca Summer School: Particles and Fields, Sao Paulo, Brazil, Feb 1997.
12. S.K. Adhikari and A. Ghosh, *J. Phys.* **A30**, 6553 (1997).
13. K.G. Richardson, M.C. Birse and J.A. McGovern, [hep-ph/9708435](#).
14. P.F. Bedaque and U. van Kolck, [nucl-th/9710073](#); P.F. Bedaque, H.-W. Hammer and U. van Kolck, [nucl-th/9802057](#).
15. U. van Kolck, Talk at Workshop on Chiral Dynamics: Theory and Experiment (ChPT 97), Mainz, Germany, Sep 1997. [hep-ph/9711222](#)
16. T.S. Park, K. Kubodera, D.P. Min and M. Rho, [hep-ph/9711463](#).
17. D.B. Kaplan, M.J. Savage and M.B. Wise, *Phys. Lett. B* **424**, 390 (1998); [nucl-th/9802075](#), to appear in *Nucl. Phys. B*;
18. J. Gegelia, [nucl-th/9802038](#).
19. J.V. Steele and R.J. Furnstahl, [nucl-th/9802069](#).
20. D.B. Kaplan, M.J. Savage and M.B. Wise, [nucl-th/9804032](#).
21. A.F. Falk, M. Luke and M.J. Savage, *Phys. Rev. D* **53**, 6316 (1996).
22. A. Manohar and H. Georgi, *Nucl. Phys. B* **234**, 189 (1984).
23. V.G.J. Stoks, R.A.M. Klomp, C.P.F. Terheggen and J.J. de Swart, *Phys. Rev. C* **49**, 2950 (1994).
24. E. Jenkins and A.V. Manohar, in *Effective Field Theories of the Standard Model*, ed. U. Meissner, World Scientific, Singapore (1992).
25. J.W. Chen, *Private Communication*.
26. J.W. Chen, H. Griebhammer, M.J. Savage and R.P. Springer, [nucl-th/9806080](#).
27. H.D. Politzer, *Nucl. Phys. B* **172**, 349 (1980).
28. C. Arzt, *Phys. Lett. B* **342**, 189 (1995).